Determination of Surface Topography and Composition of Cr-Free Pretreatment Layers on Hot Dip Galvanized Steel

Ville Saarimaa[1,*], Antti Markkula[2], Jyrki Juhanoja[1] and Bengt-Johan Skrifvars[1]

[1]*Top Analytica Oy, Ruukinkatu 4, FI-20540 Turku, Finland*

[2]*Ruukki Metals Oy, Harvialantie 420, FI-13300 Hämeenlinna, Finland*

Abstract: Topography and composition of Cr-free, titanium-based pretreatment layers on hot dip galvanized steel were studied with scanning electron microscopy, atomic force microscopy, time of flight secondary ion mass spectrometry and Auger electron spectroscopy. A layer within the target coating weight range (4-10 mg Ti/m^2) for industrial coil coating processes contained a micro-structure with hillocks and valleys, showing significant topographical variations. A local maximum film thickness of about 50 nm was detected for a sample containing 5.0 mg Ti/m^2. The hillocks were composed of metal complexes and phosphates, formed as a result of rapid zinc dissolution and metal hydroxide/phosphate precipitation reactions. During the layer formation also the polymer component of the pretreatment chemical becomes embedded within the structure. The structure composed of hillocks and valleys may be highly beneficial for paint adhesion, increasing the surface contact area for primary and secondary chemical bonding.

1. INTRODUCTION

Efficient pretreatments for hot dip galvanized (HDG) and coil coated steel should possess good adhesion properties, paintability and anti-corrosion properties against weathering and light exposure. Corrosion inhibition by conversion coating depends on the composition, structure and thickness of the coating. These parameters, together with formation of chemical bonds on the metal/organic coating interface, affect the permeability of oxygen and water [1]. Good barrier properties are essential for corrosion inhibition since they regulate the transport of ions, water and oxygen through the coating to metal surface. It still remains a challenge to achieve good corrosion protection without the use of chromates [1-4]. Transport of water and ions through the polymer coating to the polymer/pretreatment interface induces chemical changes at the interface [5]. For Cr^{6+}-containing pretreatments, these changes include the reduction of Cr^{6+} to Cr^{3+}, and the formation of a shielding Cr(OH)$_3$ barrier [6, 7]. Virtually all Cr-free pretreatments lack this effect, which means that their performance relies solely on the barrier effect built up during the layer formation, and

on the enhanced chemical bonding to paint. The barrier is supposed to prevent the zinc dissolution reactions caused by interaction with the environment [8-10]. Thus, the corrosion resistance of thin barriers is to a large extent dictated by film thickness and compactness, in addition to chemical and mechanical paint adhesion [11]. The importance of a continuous micro-barrier formation has been demonstrated for instance by in-situ corrosion potential measurements for Cr-free pretreatments [12]. Since chromates are rapidly vanishing from coil coated products, it is of great importance to expand the understanding of molecular level formation and protection mechanisms of Cr-free pretreatments. Conversion coatings based on hexafluorotitanic acids are widely being used as Cr-free alternatives for pretreatment of hot dip galvanized steel. Titanates have been shown to require integration of other components in order to reach sufficient corrosion inhibition properties [2]. A formulation based on hexafluorotitanic acid contains typically also manganese salts, phosphoric acid, hydrofluoric acid and organic polymer.

A Ti-based pretreatment layer has been characterized as an organic/inorganic hybrid film based on precipitates of metal hydroxides and phosphates embedded in an organic network [13, 14]. The formation of a conversion layer is a rapid, complex process [15-18]. The acidic pretreatment chemical

---
*Top Analytica Oy, Ruukinkatu 4, FI-20540 Turku, Finland; Tel: +358 2 282 7798; Fax: +258 2 282 7785; E-mail: Ville.Saarimaa@topanalytica.com

first mildly dissolves the zinc surface, followed by hydrogen evolution or oxygen reduction. Oxygen reduction leads to the formation of hydroxide ions. The availability of hydroxide ions initiates the acid-base precipitation of metal hydroxides, which may further dehydrate to oxides [16, 19, 20]. As a result of the pH increase, the solubility product of zinc phosphate will be exceeded, followed by precipitation. The nucleation of zinc phosphate crystals will decrease the pH and eventually cease the formation of nuclei [21, 22]. A further increase will result in formation of manganese phosphate. The interface alkalization leads also to formation of titanium oxide [12]. The presence of fluoride species in the pretreatment chemical can cause formation of zinc fluoride, ZnF_2.

Detailed structure and composition of Cr-free pretreatments on HDG have not yet been reported due to the complex structure of the deposited films [8, 13, 23]. In this study, the micro-topography and composition of Ti-based pretreatments on hot dip galvanized steel were measured using scanning electron microscopy (SEM), atomic force microscopy (AFM), time of flight secondary ion mass spectrometry (ToF-SIMS) and Auger electron spectroscopy (AES).

2. EXPERIMENTAL

2.1. Materials and Methods

Galvanized steel produced in a hot dip galvanizing line at Ruukki, Hämeenlinna, Finland, was used. The zinc substrate contained small amounts of aluminum (~0.2 wt.%). A commercial Ti-based pretreatment chemical (Henkel Granodine 1455T) was used in all tests. The main constituents of the pretreatment chemical were, according to the material safety data sheets, titanium hexafluoride, manganese salts, phosphoric acid and organic polymer (poly(4-vinyl phenol-N-glucamine)), blended together in a moderately acidic water solution (pH ~3).

2.2. Chemical Pretreatment of Coils

The laboratory pretreatments consisted of alkaline washing, rinsing with water, drying of sample, pretreatment with a laboratory roll coater, and oven drying [24]. The process-scale pretreatments were applied at Ruukki coil coating line, Hämeenlinna, Finland. The process includes two alkaline washing steps before application of pretreatment chemical by spray and squeegee technique.

2.3. Surface Characterization

SEM imaging was performed using JEOL JSM-6335F equipment. Titanium concentrations of pretreated samples were measured with an X-ray fluorescence (XRF) spectrometer (Epsilon 3, Panalytical). Atomic force microscopy (AFM) was carried out using a Nanosurf Mobile S instrument with a 100 μm scanning head. Element mapping was performed with a time of flight secondary ion mass

spectrometer (PHI Trift II). The measurements were carried out at 25 kV, 50 μm raster size and 15 min measurement time. Sputtering was done with Ga^+-ions. Element mapping was also carried out with Auger Electron Spectroscopy (AES) using a PHI 700 Auger nanoprobe at 10 kV and a beam current of 9 nA. The mapping time was about three hours.

3. RESULTS AND DISCUSSION

3.1. SEM and AFM Imaging of Pretreatment Layers

Modern Cr-free pretreatment layers on hot dip galvanized steel are typically very thin, colorless and transparent [5, 11, 12]. Thus, the main part of the pretreatment layer map analysis studies in the literature has been carried out by surface analytical techniques such as x-ray photoelectron spectroscopy (XPS), scanning Auger microprobe (SAM) and ToF-SIMS [15, 25-27]. A SEM image of a laboratory pretreated sample was taken at 2.0 kV in order to map the microstructure of the pretreatment layer (Figure **1**). The image was taken from a smooth, non-skin passed surface site. The coating weight of the pretreatment layer was 5.0 mg Ti/m². A dark web-like structure was observed on the zinc surface, potentially resembling the pretreatment layer. Thick conversion layers have been reported to be visible by SEM imaging as contrast differences, since the secondary emission yield is lower in the regions where the conversion layer is thicker [25].
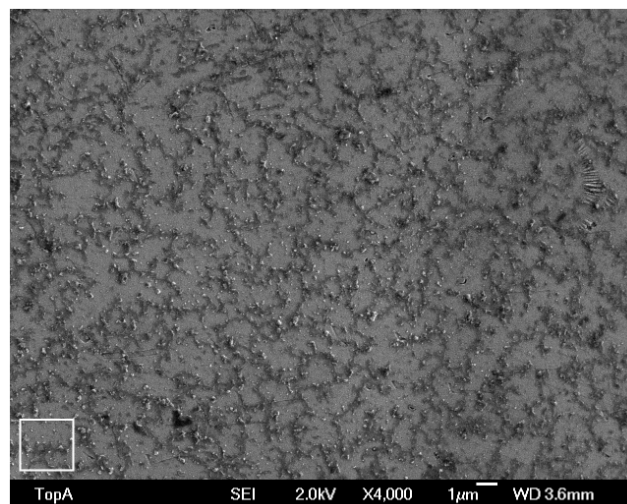
Figure 1: A SEM image of a laboratory pretreated zinc surface with 5.0 mg Ti/m². AFM image dimensions are indicated in the lower left corner.

AFM allows examination of nano -to micro-scale roughness of coatings, without requirements for electrical conductivity of the surface [28, 29]. An AFM map was recorded from the laboratory pretreated sample in order to measure the topography of the web-like structure. The AFM image size, 2.5 μm x 2.5 μm, is illustrated in the lower left corner of Figure **1**. The AFM image covered thus areas with all the different features visible in the SEM image. The AFM

topography map with three scans from selected lines (A-C) is shown in Figure **2**. In the upper line scan (A) it was observed that the layer exhibits inhomogeneous lateral thickness. The AFM line scan shows that the dark features observed in the SEM image protrude significantly from the baseline. A maximum thickness variation of 50 nm was observed. The valleys, that is the light areas in the SEM image, have more nano-scale roughness variations than the hillocks (line scans B and C, Figure **2**). Adhikari *et al.* [23] studied hexafluoro-zirconic acid –based pretreatments on cold rolled steel with AFM measurements. They observed that the deposition-induced pretreatment layer contained 10-20 nm sized nodules, which in turn formed up to 500 nm clusters, covering the surface uniformly. The overall thickness of the pretreatment was in the range of 20-30 nm. In another study a nodular structure was observed for a zirconium oxide conversion coating on hot dip galvanized steel by SEM [12]. These findings indicate that pretreatment layers are not homogeneous barriers in nanometer scale.

SEM imaging of a pretreated sample from an industrial process was also carried out in order to confirm that the observed structure was not an artifact of laboratory treated panels. A similar structure was recorded for a sample with equivalent coating weight, 5.3 mg Ti/m^2 (Figure **3**). However, the structure was tighter and the valleys (light areas) smaller than in the laboratory treated sample. The line speed was 90 m/min, much higher than in the laboratory pretreatments (<40 m/min). Also, the line pretreatment was done by spray

squeegee technique and the laboratory treatment by a roll coater. The application parameters are of great importance for the formation of the pretreatment layer. The topography of a conversion layer is reported to be highly dependent on the composition of the pretreatment chemical (and the metal substrate), since the reaction is very rapid and there is a competition between the anions (hydroxide, phosphates) and the participating metal cations (Zn^{2+}, Ti^{4+}, Mn^{2+}) [29]. In the work by Adhikari *et al.* [23] the number of nodules and clusters and the size of the clusters in the pretreatment layer increased with increasing treatment time. Wilson *et al.* [13] performed pretreatments of HDG by dipping and rinsing, followed by AFM imaging. During the initial stages of conversion layer formation, at an immersion time of 5 s, a rapid formation of islands of different sizes took place. The size of the islands depended on the immersion time and the chemical state of the zinc surface. At long immersion times, these islands merged to form an almost fully covering conversion layer. The fine structure of a pretreatment layer may thus vary greatly depending on the process conditions, affecting the chemical reactions taking place during the pretreatment layer formation.

3.2. Analysis of Pretreatment Layer Composition by ToF-SIMS and AES

The composition of the pretreatment layer was further studied by ToF-SIMS and AES. Figure **4** shows a ToF-SIMS positive total ion map and a SEM image from the same area. A mild
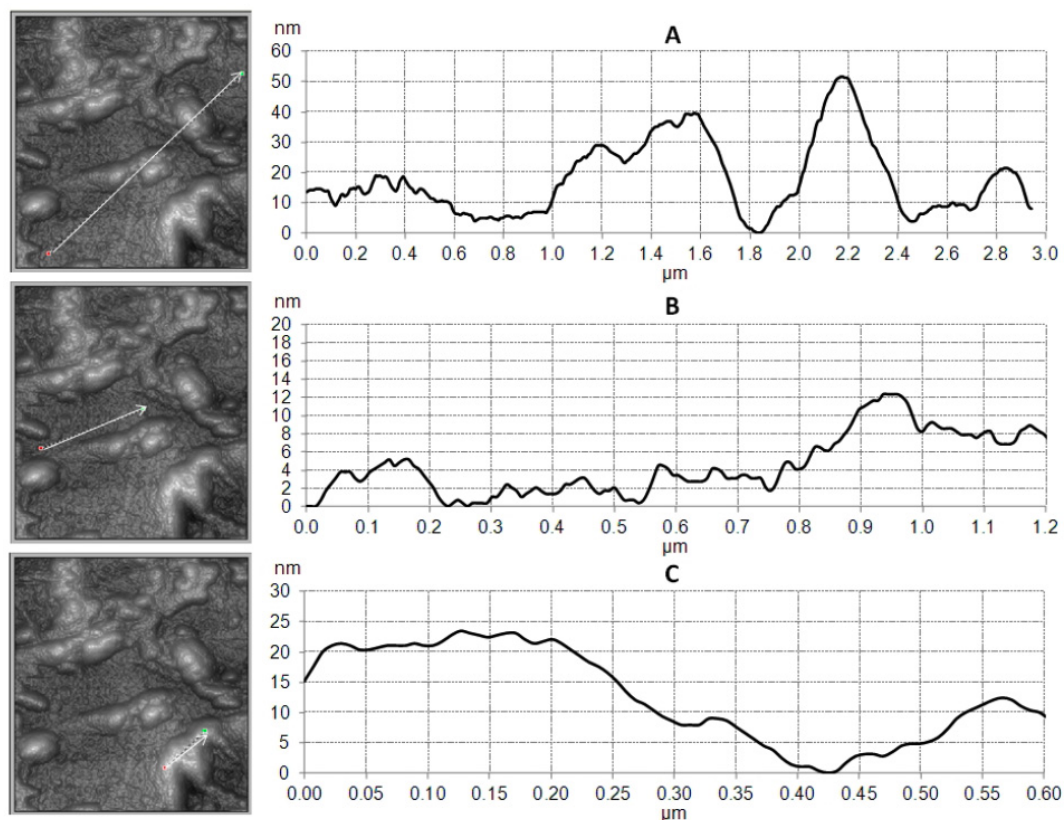
Figure 2: AFM line scans of a pretreated surface. The AFM image size is 2.5x2.5 μm.
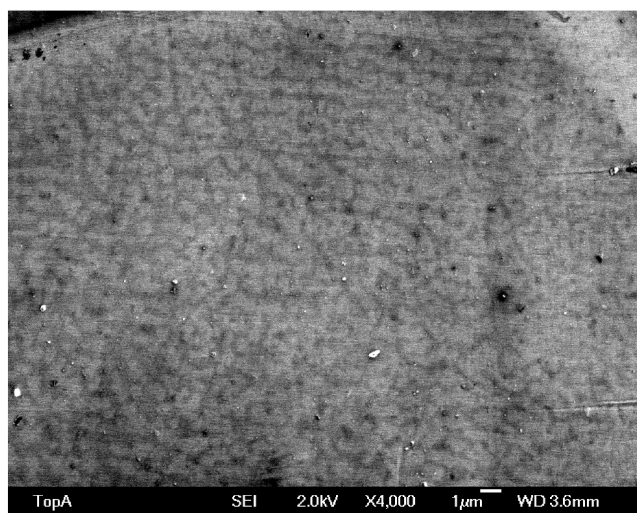
Figure 3: A SEM image of a line pretreated zinc surface with 5.3 mg Ti/m^2.

sputtering of 30 nC preceded ToF-SIMS mapping. In the ToF-SIMS image the signal intensities are strongest at the hillocks, which are the dark features in the SEM image. On the contrary, the secondary electron yield in the SEM image is strongest in the valleys (X mark). The analysis depth of ToF-SIMS is a couple of nanometers, which means that all the components contributing to the total ion intensities are derived from the top layers. Thus, based on the ToF-SIMS map there were different sputtering yields in the lateral surface of the conversion layer. The secondary electron image in the SEM analysis is gathered from a greater depth than the ToF-SIMS map. The light areas in the SEM image are a result of detection of secondary electrons from metallic zinc beneath the conversion layer. ToF-SIMS element maps from a different site of the same sample are shown in Figure **5**. Manganese and titanium maps were recorded as positive ions, while fluorine and POO maps were recorded as

negative ions. The manganese and titanium maps are practically identical. Hernández *et al*. [30] have confirmed PO$_2^-$ as a typical trace compound in phosphate-containing coatings by Raman spectroscopy. A chemically uneven surface structure of the pretreatment layer is obvious in the Mn, Ti and POO maps. Fluorine seemed to be more evenly distributed. However, ToF-SIMS is highly sensitive for fluorine. Deck *et al*. [31] suggested, based on XPS depth profiling, that most of the fluorine is enriched at the Zr-based conversion layer/metal interface, and that the ZrF$_6^{2-}$ complex is broken due to integration of Zr into oxygen-containing moieties. Berger *et al*. [15] reported sequential precipitation of different components in a Cr-free passivation solution using depth profiling by Auger electron spectroscopy.

ToF-SIMS depth profiling was also carried out. Intensity maps of Ti, Zn, C and POO at different sputtering depths are shown in Figure **6**. The titanium element maps showed a web-like structure after mild sputtering, as observed earlier. The Zn and POO element maps are similar to the Ti element map at 36 nC. Zinc was present throughout the conversion layer. The detected Zn originates in the original galvanized surface that is to some extent dissolved in the early stages of conversion layer formation in acidic conditions. Dissolved Zn is further interdispersed within the inorganic moieties of the conversion layer during the precipitation of metal hydroxides [16]. Kong *et al*. [11] observed a plateau in Zn depth profiles recorded by Auger electron spectroscopy before reaching the metallic zinc. A peak in the Zn signal intensity was visible in ToF-SIMS maps at 36 nC, indicating that zinc is indeed dissolved and precipitated during the pretreatment layer formation (Figure **6**). At the longest sputtering time most of the conversion layer was removed, revealing the underlying metallic zinc. Metallic zinc has very low secondary ion emission yield [17]. This explains why the zinc intensity is quite weak even after the conversion layer is removed. Carbon was fairly evenly distributed on the outermost
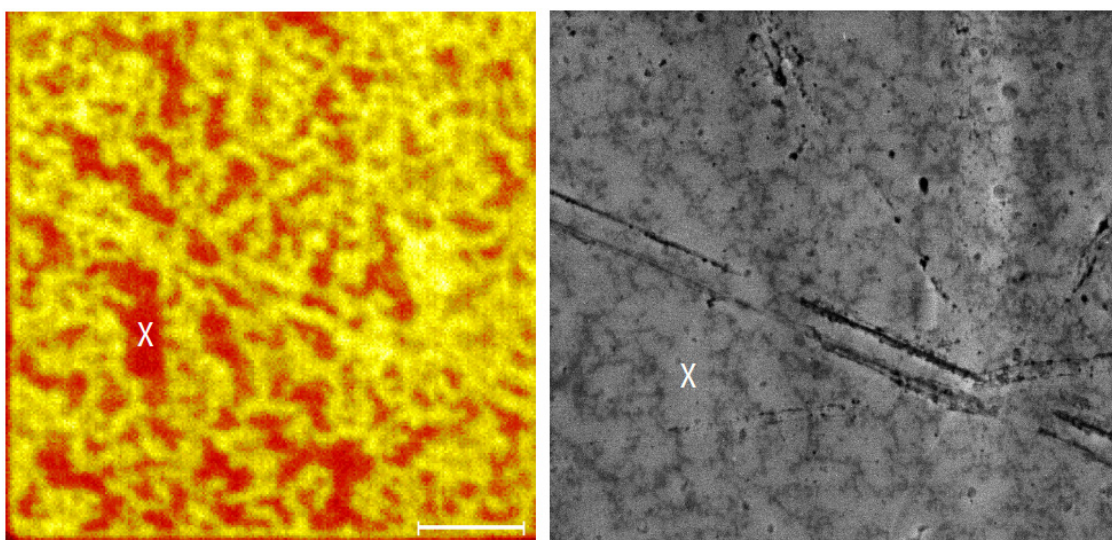
Figure 4: ToF-SIMS positive total ion map (on left) and SEM image (on right) of a laboratory pretreated sample with 2.8 mg Ti/m^2. The X mark facilitates the visual overlay of images. The image size is 50 µm x 50 µm. In the Tof-SIMS map, brighter color indicates higher signal intensity.
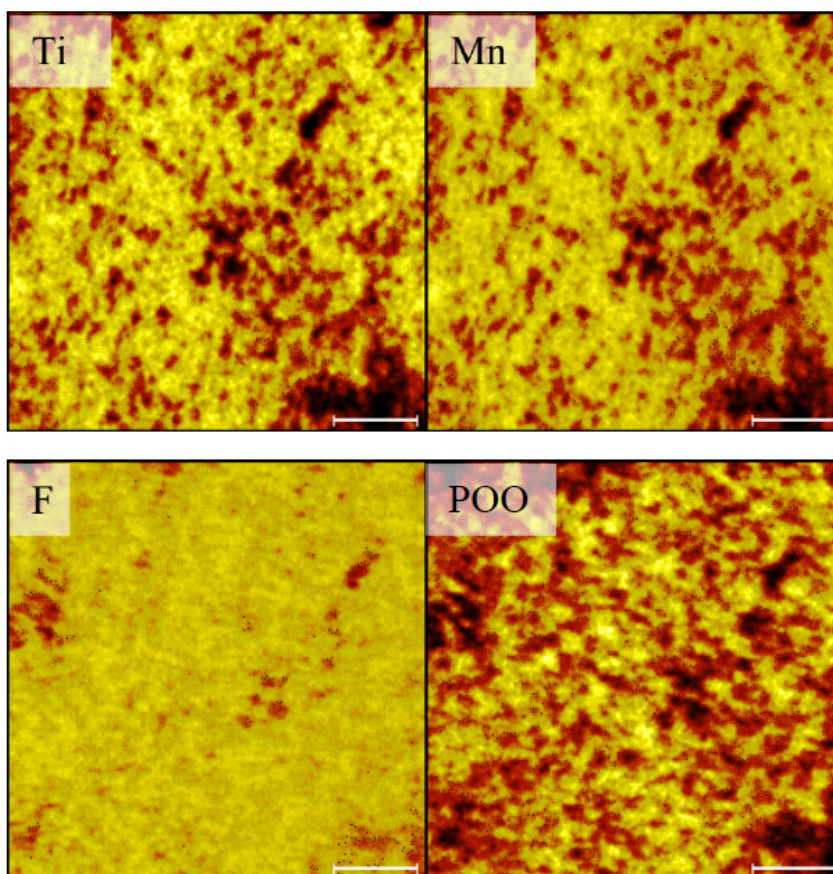
Figure 5: ToF-SIMS element maps of a laboratory pretreated sample surface recorded after mild sputtering (coating weight 2.8 mg Ti/m^2). The image size is 50 μm x 50 μm. Brighter color indicates higher signal intensity.

surface, probably largely due to surface contamination. At 36 nC, carbon was not as clearly integrated with the hillocks as Ti, Zn and POO. Phosphate intensity became stronger as the surface carbon was removed, but decreased more rapidly than titanium.

Auger electron spectroscopy provided element maps with high lateral resolution. A Zn/Ti overlay map (Figure **7**) confirmed the ToF-SIMS findings. Titanium was prominent in the hillocks of the pretreatment layer. Relatively strong zinc intensities were recorded in the areas intermediate to Ti-rich sites. AES detection depth (~10 nm) is greater than the ToF-SIMS detection depth (~2-3 nm), which explains the strong Zn signal. The AES carbon element map showed that the carbon intensity was strongest at the hillocks, originating most probably in the polymeric part of the pretreatment chemical (Figure **8**). Manchet *et al*. [26] detected carbon across the hexafluorotitanic acid-based conversion layer by XPS depth profiling. The carbon could be associated to polymeric compounds using polymer markers such as the aromatic ring and the quaternary amine group. Polymers integrated into hexafluorotitanic acid pretreatment solutions contain typically poly-(4-vinylphenol), quaternary ammonium and N-methylglucamine groups [26]. Wilson *et al*. [13] assessed kinetics of conversion layer formation on hot dip galvanized steel. The pretreatment chemical consisted of phosphoric acid, Mn, Ti and complexing organic pre-polymer. They observed a direct correlation with the build-up of phosphate-containing components and organic polymer component, which was an indication of co-deposition of these different constituents during conversion layer deposition. The research by Deck *et al*. [31] indicates that fluorotitanic acid operates as a cross linker between the polymer and the metal surface. The presence of manganese phosphate species also seems to promote polymer adsorption on the HDG surface [26].

It is thus confirmed that the analyzed pretreatment layer does not have homogeneous thickness. At the valleys the zinc surface is covered only by a thin few nanometer carbon layer, which may be largely due to surface contamination [11].

3.3. Potential Effects of the Pretreatment Layer Microstructure

Pretreatment layer thickness values from depth profiles obtained with glow discharge optical emission spectroscopy (GDOES) [5, 25, 32], AES [15, 33] and XPS [13] are inherently estimations, since the pretreatment layer/metal surface interface has to be manually set based on the shape of the element profiles. In the light of this study, in addition to macroscopic roughness variations of the galvanized steel, also the microstructure of the deposited pretreatment layer
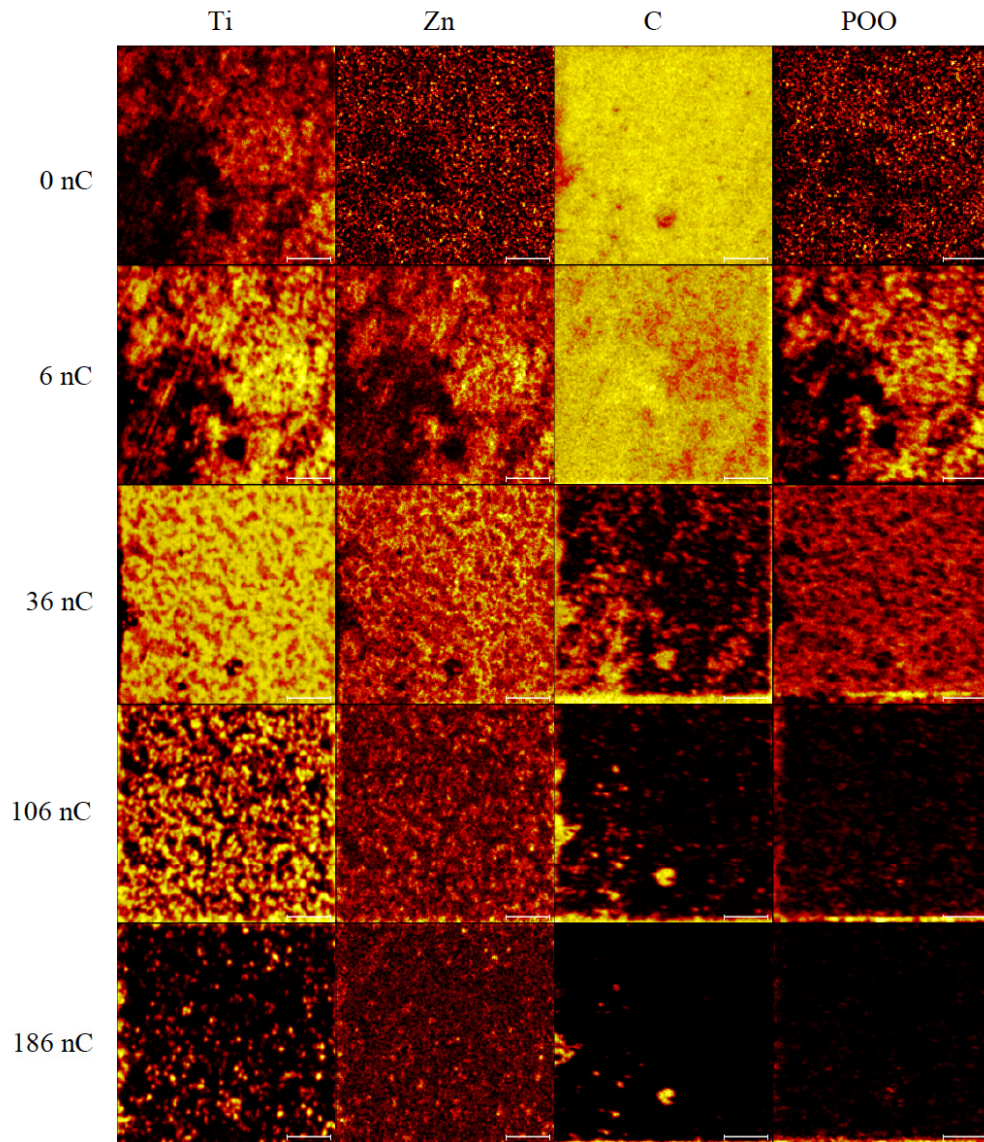
Figure 6: ToF-SIMS element maps of Ti, Zn, C and POO at different sputtering depths for a laboratory pretreated sample (laboratory pretreated sample, 2.8 mg Ti/m^2). The image size is 50 µm x 50 µm. Brighter color indicates higher signal intensity.
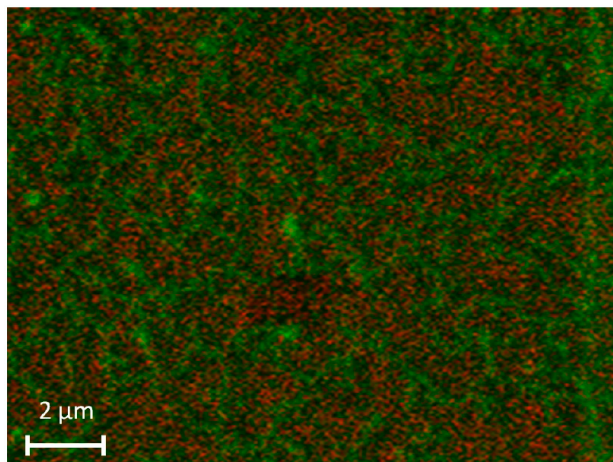
Figure 7: An overlay map of Zn (red) and Ti (green) maps recorded with Auger electron spectroscopy from a laboratory pretreated sample with 5.0 mg Ti/m^2.
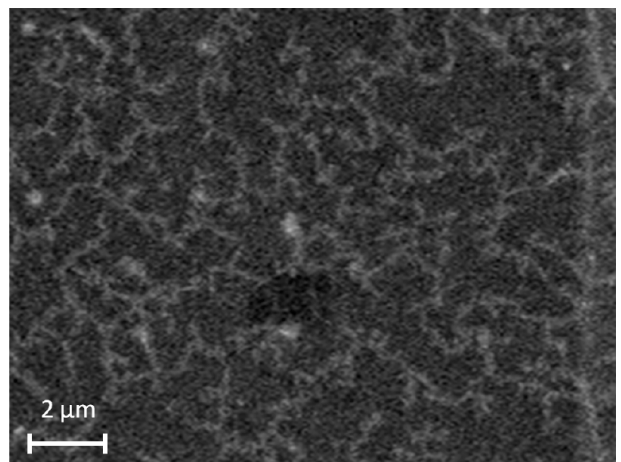
Figure 8: A carbon element map recorded with Auger electron spectroscopy from a laboratory pretreated sample with 5.0 mg Ti/m^2.

strongly affects the element depth profiles. At the valleys of the pretreatment layer the sputtering can immediately bring about high zinc signal, while it still takes some time to peel off the protruding hillocks of the coating. This may render the interpretation of the pretreatment layer composition at different sputtering depths challenging.

Adhesion is generally considered comprising of three components: primary chemical bonding (ionic or covalent bonding), secondary (polar) bonding and mechanical bonding. Conversion coatings are mainly dependent on primary chemical bonding. Paints mainly rely on secondary chemical bonding that is polar interactions like hydrogen bonds and van der Waals forces [3]. It has been shown by detailed AFM and transmission electron microscopy/x-ray energy dispersive spectrometry (TEM/EDX) analysis of chromate pretreatment films that a nano-porous surface increases the number of interfacial bonding sites [22]. A micro-rough pretreatment layer may thus increase the specific surface area for chemical paint adhesion.

4. CONCLUSIONS

Hexafluorotitanic acid-based pretreatment chemical was applied on hot dip galvanized steel with careful laboratory practice. The pretreatment layer micro-topography and structure were analyzed by SEM and AFM. The pretreatment layer was composed of micro-scale hillocks and valleys. Thickness variations of 50 nm were recorded for a smoothly applied pretreatment layer containing 5.0 mg Ti/m^2. A similar structure was also detected in a sample with lower pretreatment coating weight (2.8 mg Ti/m^2) and in a line pretreated sample with 5.3 mg Ti/m^2. ToF-SIMS and AES are versatile analysis techniques with surface sensitive imaging and depth profiling capabilities. ToF-SIMS and AES analyses showed that the pretreatment layer was composed of an organic/inorganic structure containing hillocks and valleys. Zinc, manganese, titanium, phosphates and carbon were prominent in the hillocks of the pretreatment layer. Only a thin carbon layer was covering the valleys of the layer. Phosphates were more prominent on the surface of the layer, while Zn, Mn and Ti compounds were more equally distributed throughout the layer. Carbon-containing organic moieties, resembling the polymer constituent of the pretreatment chemical, were precipitated with the metal oxide/hydroxide and phosphate structure. The observed topographical and compositional variations in the pretreatment layer may improve secondary chemical bonding to paint by increasing the surface contact area. Hexafluorotitanic acid-based pretreatments are thin layers with nanoscale physicochemical features that require sophisticated analytical tools to be assessed. It is of utmost importance to control the parameters affecting the formation of Ti-based pretreatment layers, since they lack the self healing properties of chromates and operate mainly *via* barrier formation and by enhancing chemical bonding to paint.

REFERENCES

[1]   Marcus P, Ouder J, Eds. Corrosion Mechanisms in Theory and Practise. New York: Marcel Dekker 1995.

[2]   Yang H, Kong X, Lu W, Liu Y, Guo J, Liu S. High anticorrosion chromate-free passivate films made by titanate and waterborne polyurethane on galvanized steel sheet. Prog Org Coat 2010; 67: 375-80.
http://dx.doi.org/10.1016/j.porgcoat.2010.01.001

[3]   Zhang J. Development of environmentally friendly non-chrome conversion coatings for cold-rolled steel [PhD thesis]. Blacksburg, Virginia Polytechnic Institute and State University; 2003.

[4]   Jašková V, Kalendová A. Anticorrosive coatings containing modified phosphates. Prog Org Coat 2011; 75: 328-34.
http://dx.doi.org/10.1016/j.porgcoat.2012.07.019

[5]   Öhman M, Persson D, Jacobsson D. In situ studies of conversion coated zinc/polymer surfaces during exposure to corrosive conditions. Prog Org Coat 2011; 70:16-22.
http://dx.doi.org/10.1016/j.porgcoat.2010.09.012

[6]   Zhang X, Sloof WG, Hovestad A, van Westing EP, Terryn H, de Wit JH. Characterization of chromate conversion coatings on zinc using XPS and SKPFM. Surf Coat Tech 2005; 197: 168-76.
http://dx.doi.org/10.1016/j.surfcoat.2004.08.196

[7]   Freeman DB. Phosphating and metal pre-treatment. Great Britain: Woodhead-Faulkner; 1986.

[8]   Ogle K, Morel S, Meddahi N. An electrochemical study of the delamination of polymer coatings on galvanized steel. Corros Sci 2005; 47: 2034-52.
http://dx.doi.org/10.1016/j.corsci.2004.08.017

[9]   Jiang L, Wolpers M, Volovitch P, Ogle K. An atomic emission spectroelectrochemical study of passive film formation and dissolution on galvanized steel treated with silicate conversion coatings. Surf Coat Tech 2012; 206: 3151-7.
http://dx.doi.org/10.1016/j.surfcoat.2012.01.016

[10]   De Graeve I, Schoukens I, Lanzutti A, *et al*. Mechanism of corrosion protection of hot-dip aluminium–silicon coatings on steel studied by electrochemical depth profiling. Corros Sci 2013; 76: 325-36.
http://dx.doi.org/10.1016/j.corsci.2013.07.005

[11]   Kong G, Lu J, Zhang S, Che C, Wu H. A comparative study of molybdate/silane composite films on galvanized steel with different treatment processes. Surf Coat Tech 2010; 205: 545-50.
http://dx.doi.org/10.1016/j.surfcoat.2010.07.033

[12]   Lostak T, Krebs S, Maljusch A, Gothe T, Giza M, Kimpel M, Flock J, Schulz S. Formation and characterization of Fe^{3+}/Cu^{2+}-modified zirconium oxide conversion layers on zinc alloy coated steel sheets. Electrochim Acta 2013; 112: 14-23.
http://dx.doi.org/10.1016/j.electacta.2013.08.161

[13]   Wilson B, Fink N, Grundmeier G. Formation of ultra-thin amorphous conversion films on zinc alloy coatings: Part 2: Nucleation, growth and properties of inorganic–organic ultra-thin hybrid films. Electrochim Acta 2006; 51: 3066-75.
http://dx.doi.org/10.1016/j.electacta.2005.08.041

[14]   Posner R, Fink N, Wolpers M, Grundmeier G. Electrochemical electrolyte spreading studies of the protective properties of ultra-thin films on zinc galvanized steel. Surf Coat Tech 2013; 228: 286-95.
http://dx.doi.org/10.1016/j.surfcoat.2013.04.042

[15]   Berger R, Bexell U, Grehk TM, Hörnström SE. A comparative study of the corrosion protective properties of chromium and chromium free passivation methods. Surf Coat Tech 2007; 202: 391-7.
http://dx.doi.org/10.1016/j.surfcoat.2007.06.001

[16]   Zhu L, Yang F, Ding N. Corrosion resistance of the electro-galvanized steel treated in a titanium conversion solution. Surf Coat Technol 2007; 201: 7829-34.
http://dx.doi.org/10.1016/j.surfcoat.2007.03.024

[17] Berger R, Bexell U, Stavlid N, Grehk TM. The influence of alkali-degreasing on the chemical composition of hot-dip galvanized steel surfaces. Surf Interface Anal 2006; 38: 1130-8.
http://dx.doi.org/10.1002/sia.2364

[18] Nordlien JH, Walmsley JC, Østerberg H, Nisancioglu K. Formation of a zirconium-titanium based conversion layer on AA 6060 aluminium. Surf Coat Tech 2002; 153: 72-8.
http://dx.doi.org/10.1016/S0257-8972(01)01663-2

[19] Volovitch P, Allely C, Ogle K. Understanding corrosion *via* corrosion product characterization: I. Case study of the role of Mg alloying in Zn-Mg coating on steel. Corros Sci 2009; 51: 1251-62.
http://dx.doi.org/10.1016/j.corsci.2009.03.005

[20] Tsai YT, Hou KH, Bai CY, Lee JL, Ger MD. The influence on immersion time of titanium conversion coatings on electrogalvanized steel. Thin Solid Films 2010; 518: 7541-4.
http://dx.doi.org/10.1016/j.tsf.2010.05.042

[21] Tegehall PE, Vannerberg NG. Nucleation and formation of zinc phosphate conversion coating on cold-rolled steel. Corros Sci 1991; 32: 635-52.
http://dx.doi.org/10.1016/0010-938X(91)90112-3

[22] Matsuzaki A, Yamashita M, Hara N, Effect of pretreatment film composition on adhesion of organic film on zinc coated steel sheet. Mater Trans 2010; 51: 1833-41.
http://dx.doi.org/10.2320/matertrans.M2010185

[23] Adhikari S, Unocic KA, Zhai Y, Frankel GS, Zimmerman J, Fristad W. Hexafluorozirconic acid based surface pretreatments: Characterization and performance assessment. Electrochim Acta 2011; 56: 1912-24.
http://dx.doi.org/10.1016/j.electacta.2010.07.037

[24] Saarimaa V, Kauppinen E, Markkula A, Juhanoja J, Skrifvars BJ, Steen P. Microscale distribution of Ti-based conversion layers on hot dip galvanized steel. Surf Coat Tech 2012; 206: 4173-9.
http://dx.doi.org/10.1016/j.surfcoat.2012.04.017

[25] Lunder O, Simensen C, Yu Y, Nisancioglu K. Formation and characterization of Ti-Zr based conversion layers on AA6060 aluminum. Surf Coat Tech 2004; 184: 278-90.
http://dx.doi.org/10.1016/j.surfcoat.2003.11.003

[26] Le Manchet S, Verchère D, Landoulsi J. Effects of organic and inorganic treatment agents on the formation of conversion layer on hot-dip galvanized steel: An X-ray photoelectron spectroscopy study. Thin Solid Films 2012; 520: 2009-16.
http://dx.doi.org/10.1016/j.tsf.2011.09.064

[27] Bexell U. Surface Characterization Using ToF-SIMS, AES and XPS of Silane Films and Organic Coatings Deposited on Metal Substrates [PhD Thesis]. Sweden. Uppsala University; 2003.

[28] Bierwagen GP, Twite R, Chen G, Tallman DE. Atomic force microscopy, scanning electron microscopy and electrochemical characterization of Al alloys, conversion coatings, and primers used for aircraft. Prog Org Coat 1997; 32: 25-30.
http://dx.doi.org/10.1016/S0300-9440(97)00097-0

[29] Rezaee N, Attar MM, Ramezanzadeh B. Studying corrosion performance, microstructure and adhesion properties of a room temperature zinc phosphate conversion coating containing Mn^{2+} on mild steel. Surf Coat Tech 2013; 236: 361-7.
http://dx.doi.org/10.1016/j.surfcoat.2013.10.014

[30] Hernández M, Genescá J, Uruchurtu J, Galliano F, Landolt D. Effect of an inhibitive pigment zinc-aluminum-phosphate (ZAP) on the corrosion mechanisms of steel in waterborne coatings. Prog Org Coat 2006; 56: 199-206.
http://dx.doi.org/10.1016/j.porgcoat.2006.05.001

[31] Deck PD, Moon M, Sujdak RJ. Investigation of fluoacid based conversion coatings on aluminium. Prog Org Coat 1998; 34: 39-48.
http://dx.doi.org/10.1016/S0300-9440(98)00017-4

[32] Puomi P, Fagerholm HM, Rosenholm JB, Jyrkäs K. Comparison of different commercial pretreatment methods for hot-dip galvanized and Galfan coated steel. Surf Coat Tech 1999; 115: 70-8.
http://dx.doi.org/10.1016/S0257-8972(99)00170-X

[33] Critchlow GW, Brewis DM. A comparison of chromate-phosphate and chromate-free conversion coatings for adhesive bonding. J Adhesion 1997; 61: 213-30.
http://dx.doi.org/10.1080/00218469708010523